Nitric acid phase partitioning and cycling in the New England coastal atmosphere

E. Fischer,[1] A. Pszenny,[1,2] W. Keene,[3] J. Maben,[3] A. Smith,[3] A. Stohl,[4] and R. Talbot[5]

[1]   During summer 2004, HNO_3 and size-resolved aerosols were measured in parallel, and corresponding dry-deposition fluxes were modeled at Appledore Island, Maine, as part of the International Consortium for Atmospheric Research on Transport and Transformation (ICARTT) field program. HNO_3 concentrations varied widely on the timescale of hours; however, all days were characterized by a minimum near sunrise. Mixing ratios normally peaked in the early afternoon; maximum and median concentrations of HNO_3 during the campaign were 337 and 22.8 nmol m^{-3}, respectively. Aerosol NO_3^- exhibited a bimodal size distribution with a primary peak associated with sea salt at $\sim$4 μm and a secondary sub-μm peak. The median NO_3^- concentrations in sub- and super-μm diameter size fractions were 3.3 and 7.7 nmol m^{-3}, respectively. Peak HNO_3 and super-μm NO_3^- concentrations were associated with westerly and southwesterly flow regimes respectively. The multiphase cycling of HNO_3 was evaluated as a function of transport sector. Although median total nitrate ($HNO_3 + NO_3^-$) concentrations were higher under westerly flow, higher median dry-deposition rates of total nitrate were associated with southwesterly flow. Sea-salt concentrations were $\sim$3 times greater during southwesterly flow, which shifted the phase partitioning toward particulate NO_3^-. Consequently, under westerly flow, HNO_3 deposited more quickly than aerosol NO_3^-, while for southwesterly flow, the fluxes from the two phases were comparable. On the basis of all data, the median dry-deposition fluxes for HNO_3 and aerosol NO_3^- were 8.2 and 5.6 μmol m^{-2} d^{-1}; super-μm size fractions dominated the NO_3^- flux.

1.   Introduction

[2]   Increases in energy and food production over the last century have resulted in human dominance of the terrestrial nitrogen (N) cycle, especially the production of reactive N [*Galloway and Cowling*, 2002]. The New England coast and the Gulf of Maine are located downwind of substantial anthropogenic atmospheric N sources, including sources from both urban and agricultural sectors [*U.S. Environmental Protection Agency* (*U.S. EPA*), 2002]. Significant atmospheric, ecological, and human health consequences have resulted from elevated N input to the Northeast, including increased tropospheric ozone, the alteration of forest nitrogen and carbon cycles, the acidification of terrestrial soils and surface waters, and the eutrophication of estuaries and adjacent coastal waters [*Driscoll et al.*, 2003].

[3]   Atmospheric deposition is one of many sources of N to coastal ecosystems in the Gulf of Maine, but comprehensive investigations of all major sources are rare and consequently, the relative importance of atmospheric deposition is uncertain. Available evidence suggests that, relative to dry deposition, wet deposition delivers greater amounts of oxidized N to the eastern U.S. coastal zone [*Castro et al.*, 2001]. Previous measurements at a Gulf of Maine coastal site indicate that the dry-deposition of particulate nitrate (NO_3^-) and gaseous nitric acid (HNO_3) contribute significantly to the total deposition fluxes of atmospheric N, and the flux of particulate ammonium (NH_4^+) is relatively unimportant [*Jordan and Talbot*, 2000]. However, this study did not consider contributions from the dry deposition of ammonia (NH_3), which dominates dry-deposition fluxes of atmospheric N to the mid-Atlantic coastal zone [*Russell et al.*, 2003].

[4]   With respect to the N budget for the entire Gulf of Maine, atmospheric deposition is a minor pathway [*Schlitz and Cohen*, 1984], contributing $\leq$5% of the input flux of reactive N. The main source of reactive N to surface waters in the Gulf of Maine is the upwelling of nutrient-rich deep

[1]Mount Washington Observatory, North Conway, New Hampshire, USA.
[2]Also at Institute for the Study of Earth, Oceans, and Space, University of New Hampshire, Durham, New Hampshire, USA.
[3]Department of Environmental Sciences, University of Virginia, Charlottesville, Virginia, USA.
[4]Norwegian Institute for Air Research, Kjeller, Norway.
[5]Institute for the Study of Earth, Oceans, and Space, University of New Hampshire, Durham, New Hampshire, USA.
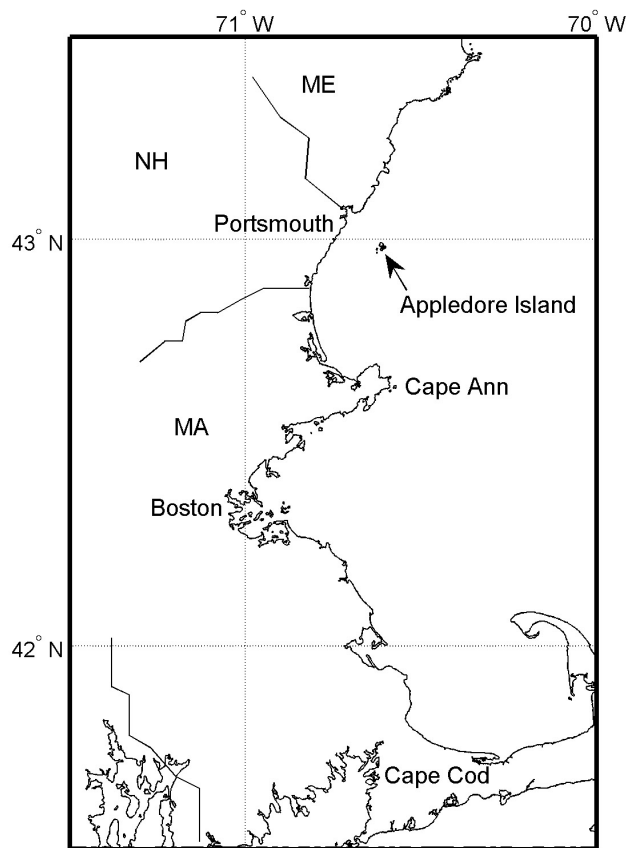
Figure 1. Location of the sampling site at Appledore Island, Maine.

ocean water [*Townsend*, 1998]. However, this upwelling is seasonal and during the summer months stratification [*Brooks*, 1985] can isolate surface waters from the deep-water nutrient sources over much of the Gulf [*Bisagni*, 2003]. During this time of year, the episodic direct deposition of atmospheric N may enhance the productivity of the Gulf of Maine [*Jordan et al.*, 2000].

[5] The response of aquatic ecosystems to atmospheric N deposition varies as a function of the timing, the spatial distribution and the relative amounts of the nutrients deposited [*Paerl*, 1988, 1997]. Coastal eutrophication resulting from the atmospheric deposition of N is manifested most visibly as algal blooms, [*Paerl and Witall*, 1999], although hypoxic and anoxic bottom waters, loss of sea grasses, and reduced fish stocks are other common symptoms [*Castro et al.*, 2001]. Episodic events of atmospheric N deposition have been shown to make an important contribution to new production in aquatic ecosystems [*Owens et al.*, 1992]. The chemical speciation of N entering an ecosystem is also important because it can influence the composition and size distribution of algal communities [*Stolte et al.*, 1994].

[6] Within New England most NO_x ($NO + NO_2$) is emitted to the atmosphere from on-road vehicles (57%), off-road vehicles (20%), large industry and electric utilities (13%) and smaller combustion sources in the commercial and residential sectors (10%) [*U.S. EPA*, 2002]. Atmospheric N is also regularly transported into the Northeast from

sources in the Midwest, the mid-Atlantic, and southern Canada [*Driscoll et al.*, 2003], and thus changing synoptic flow patterns bring air masses of various origins and physiochemical properties to this coastal region [*Jordan et al.*, 2000]. Previous work in the region indicates that the greatest concentrations of anthropogenic pollutants arrive from the southwest and westerly sectors, and relatively clean air arrives from the northwest and northerly sectors [*Moody et al.*, 1998; *Lefer and Talbot*, 2001].

[7] The sea breeze and local-scale meteorology are superimposed on the synoptic transport, and play important roles in determining weather [*Miller and Keim*, 2003] and pollutant concentrations near the New England coast [*Angevine et al.*, 1996a, 1996b; *Ray et al.*, 1996]. The marine boundary layer (MBL) in this region is shallow, approximately 100 m, and during summer is extant during all periods of offshore flow [*Angevine et al.*, 2005]. Strong vertical wind shear and a stable atmosphere over the ocean cause heavily polluted plumes advected from the Boston and New York City urban areas to break apart into confined air parcels as they move out over the Gulf of Maine [*Senff et al.*, 2005]. The extent to which the export of these plumes, and the NO_x emissions they contain, impact the composition of the MBL is a topic of current research.

[8] During summer 2004 the evolution of air pollutants over New England and the Gulf of Maine was investigated on the basis of coordinated meteorological and chemical measurements at land sites, aircraft and ship platforms as part of the International Consortium for Atmospheric Research on Transport and Transformation (ICARTT) field program. This study focuses on the multiphase cycling and deposition of HNO_3 at Appledore Island, Maine.

2. Methods

2.1. Site Description and Sampling Times

[9] Between 6 July and 12 August 2004, soluble gases and size resolved aerosols were sampled from the top of an aluminum scaffolding tower section affixed to the roof of a ~40 m WWII-era surveillance tower on Appledore Island, Maine (42°59'13.5"N, 70°23'55.4"W, ~0.39 km^2), located approximately 10 km off the shore of New Hampshire (Figure 1). Samples were processed in a temporary laboratory set up in space provided by the Shoals Marine Laboratory on the island. The laboratory housed clean benches, a deionized water system, ion chromatographs, and other related equipment. A 3-day break in sampling occurred from 23 to 25 July.

2.2. Sampling

2.2.1. Aerosols

[10] Size-segregated aerosols were sampled continuously over discrete daytime (~15 hr) or nighttime (~9 hr) intervals using modified (with the addition of a top "0" stage) Graseby-Anderson 235 cascade impactors, with a Liu-Pui type inlet, polycarbonate impaction substrates and quartz-fiber backup filters (Palliflex 2500 QAT-UP) [*Keene et al.*, 2004]. Bulk aerosols were collected in parallel with quartz-fiber filters. Flow rates through the bulk filters and cascade impactors were monitored using separate sharp-edged orifice flow tubes that were calibrated in situ using a NIST-traceable Tisch static-pressure device; the average

sampling rates for impactor and bulk aerosol sampling were 1.0 and 1.2 m^3 min^{-1}, respectively. All air volumes reported herein were adjusted to standard temperature ($0°C$) and pressure (1 atm). The mean 50% aerodynamic cut diameters for the sampled resolved aerosol size fractions were 18, 9.9, 3.9, 2.2, 1.1, 0.56, 0.28 μm. The mean diameter for the smallest size fraction was estimated as half of the diameter of the next largest stage. A total of 60 pairs of size-resolved and bulk aerosol samples were collected (30 daytime and 30 nighttime) along with 7 blanks. Dynamic field blanks were mounted on the collection instruments, and exposed by drawing ambient air through them for 1 min. The field blanks were then processed and analyzed following the same procedures used for the samples. Aerosol sampling was suspended during infrequent precipitation and heavy fog events.

[11] Impactors and bulk-filter cassettes were cleaned, dried, loaded, and unloaded in a Class 100 clean bench. Following collection, the substrates were halved and transferred to high-density polyethylene extraction vials, which were sealed inside cleaned glass mason jars to minimize gas exchange. Samples were frozen and transported in insulated coolers to the Mount Washington Observatory (MWO) for chemical analysis.

2.2.2. HNO$_3$

[12] Soluble gases were sampled continuously over 2-hour intervals using tandem mist chambers containing 20 mL of deionized water (DIW) at flow rates of $\sim$15 L min^{-1} [Keene et al., 2004]. Flow rates through the mist chambers were monitored with Teledyne-Hastings mass flowmeters that had been factory calibrated prior to the experiment. Flowmeters were intercompared immediately before the experiment (agreed within ±1%) and after the experiment (agreed within ±1–3%). The air was sampled through a size-fractioning inlet that removed super-μm diameter aerosol from the sample stream [Keene et al., 1993]; sub-μm aerosol was removed downstream by an inline Teflon filter (Zefluor 2 μm). Inline filters were changed approximately every 2 days. All components of the inlet upstream of the mist chambers were fabricated of PFA Teflon. To minimize surface losses, sample lines between the inlet and each filter/chamber assembly were passivated with 20% H_3PO_4 in acetone and were made as short as possible (average $\sim$50 cm). Immediately preceding each period of sequential sampling, the inlet and sample lines were conditioned by flushing with ambient air for about 2 hours. Passing efficiencies for HNO$_3$ were determined in the laboratory over a representative range of mixing ratios and with and without sea salt coatings. These results indicate passing efficiencies of essentially 100% for a clean inlet and about 86% for a heavily salted inlet [Keene et al., 2004]. The broad dynamic ranges in measured HNO$_3$ mixing ratios and, in particular, the rapid decreases from high to near detection-limit concentrations during some periods (see below), suggest that sub-μm aerosols collected on the inline filter remained at near equilibrium with the ambient gas phase and, consequently, did not significantly dampen (via evaporation or condensation) variability in measured relative to ambient HNO$_3$. A total of 311 samples were collected along with 25 blanks.

2.3. Analytical Techniques
2.3.1. Aerosols

[13] Half sections of the polycarbonate substrates were extracted in 13 mL DIW with vigorous shaking by hand (1 min) and with a mini vortexer (30 s) followed by 20 min of sonication and an additional minute of vigorous shaking. Half sections of the quartz filters were extracted in 40 mL DIW with a similar shaking and sonicating procedure. The quartz extracts were then filtered through prerinsed 13 mm 0.45 μm PTFE membrane filters. Aliquots of the extracts were analyzed by ion chromatography as soon as possible after extraction (usually within 12 hours). Concentrations of NO_3^-, Cl^-, SO_4^{2-} and other anions were analyzed with a Dionex IC25 equipped with an AS15 column and a KOH eluent gradient ranging from 8 to 50 mM. Na^+ and other cations were analyzed with a Dionex IC25 equipped with a CS12A column and 20 mM methanesulfonic acid eluent. Concentrations in sample extracts were corrected on the basis of the median concentrations of the blank extracts. Sea-salt and non-sea-salt (nss) constituents were differentiated using Na^+ as the sea-salt reference species [Keene et al., 1986]. Typical internal losses of super-μm aerosols in the type of cascade impactor used are 25–30% [Willeke, 1975; Russell et al., 2003]. Other sources of bias for size-resolved aerosol measurements using cascade impactors are considered negligible [Keene et al., 1990].

2.3.2. HNO$_3$

[14] Within 12 hours after collection, NO_3^- in the mist chamber solution was analyzed on site by ion chromatography using a Dionex IC25, with an AS15 column and a KOH eluent gradient ranging from 8 to 50 mM. Sample data were corrected on the basis of the median values for the field blanks. The average estimated detection limit for HNO$_3$ was 27 pptv and the average estimated precision was ±13 pptv or ±10% which ever was the greater absolute value [Keene et al., 1989].

2.4. Meteorological Measurements

[15] Wind direction, wind speed, air temperature, and relative humidity (RH) measured at the National Data Buoy Center C-MAN station (IOSN3) located on White Island (13 m above mean sea level, 42°58'00″ N, 70°37'24″ W), approximately 2.3 km south of Appledore Island tower were used in this analysis. The NOAA Earth System Research Laboratory (ESRL) also operated a wind profiler on Appledore Island, which provided hourly wind information up to 4000 m (http://www.profiler.noaa.gov/npn/profiler.jsp).

2.5. Dry-Deposition Flux Calculations

[16] Dry-deposition velocities (V_d) for size-resolved aerosols to the ocean surface were modeled on the basis of the measured chemical composition and geometric mean diameter for each size fraction, RH, temperature, and wind speed following Hummelshoj et al. [1992]; 98% RH was assumed for the laminar sublayer [Hummelshoj et al., 1992; Lewis and Schwartz, 2004]. In this model, particle diameter and wind speed are the most important parameters controlling the deposition velocity. V_d for HNO$_3$ to the ocean surface was modeled using a bulk exchange method that determines the turbulent fluxes of heat, moisture, and momentum over water. This method requires measurements of wind speed and air and surface-seawater temperatures to model V_d

[*Valigura*, 1995]. A general review of the assumptions required for these calculations is provided by [*Hicks*, 1975] and [*Liu and Schwab*, 1987]. *Valigura* [1995] anticipates that this method is likely conservative because it does not account for the scavenging of HNO_3 by aerosol particles or water droplets. *Valigura* [1995] also notes that inhomogeneous meteorological conditions along the coast and very low wind speeds may violate assumptions of this model. The flux (F_s) of a gaseous or particulate species to the water surface is defined as:

$$F_s = V_d C_s, \qquad (1)$$

where C_s is the atmospheric concentration at 10m above the water surface. This approach assumes no vertical gradient between the reference height of 10 m and the sampling height of ∼40 m.

2.6. Atmospheric Transport

[17] Column residence time and footprint residence plots provided by NOAA Chemical Sciences Division (http://www.al.noaa.gov/ICARTT/analysis/) and HYSPLIT trajectories archived at Plymouth State University (http://pscwx.plymouth.edu/ICARTT/archive.html) were visually inspected to create six regional flow regime classifications. To generate the column residence time and footprint residence plots, the particle dispersion model FLEXPART [*Stohl et al.*, 1998, 2005] was run in backward mode [*Stohl et al.*, 2003; *Seibert and Frank*, 2004] in order to see where the sampled air masses were potentially exposed to emissions. FLEXPART was driven with ECMWF analyses of 0.36° resolution and accounts for turbulence and deep convection, in addition to the transport by grid-resolved winds. Every 3 hours, 40000 particles were released from the location of the measurement site and followed backward in time for 20 days to calculate a so-called potential emission sensitivity (PES) function, as described by *Seibert and Frank* [2004] and *Stohl et al.* [2003]. The word "potential" here indicates that this sensitivity is based on transport alone, ignoring removal processes that otherwise would reduce the sensitivity. The value of the PES function (in units of s kg^{-1}) in a particular grid cell (resolution 0.25° latitude × 0.333° longitude) is proportional to the particle residence time in that cell. It is a measure for the mixing ratio at the sampling site that a source of unit strength (1 kg s^{-1}) in the respective grid cell would produce. Of special interest is the PES distribution at altitudes where emissions are likely to occur. Here, results will be presented for a so-called footprint layer of 150 m above ground. The PES integrated over the entire atmospheric column also gives a good visualization of the pathway an air mass has taken, similar to classical back trajectories.

[18] Folding (i.e., multiplying) the PES footprint with the distribution of actual emission flux densities (in units of kg m^{-2} s^{-1}) from an emission inventory yields a so-called potential source contribution (PSC) map, that is the geographical distribution of sources contributing to the simulated mixing ratio at the receptor. Spatial integration of the PSC map finally gives the simulated mass mixing ratio at the receptor. For the emission distribution, the inventory of *Frost et al.* [2006] with a base resolution of
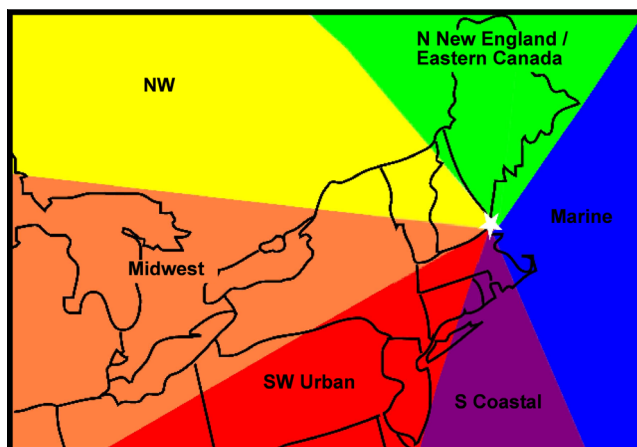

Figure 2. Six major regions of influence. This color scheme is also used in Figures 5 and 6. The classification scheme does not account for mesoscale transport such as the land sea breeze.

4 km, remapped to the 0.25° × 0.333° resolution of the PES output, was used [*Frost et al.*, 2006].

[19] The HYSPLIT trajectories [*Draxler and Rolph*, 2005] were initialized from 10, 500, and 1000 meters above ground level every 6 hours using the North American Mesoscale (NAM) 12 km analysis. Over-water transit times from the coast to Appledore Island were estimated using 36-hour back trajectories calculated from the NOAA ESRL profiler network and ocean buoy data (http://www.etl.noaa.gov/data/profiler_data/processed/ProfilerTrajectory/). Sampling periods influenced by a local sea breeze were assessed using the NOAA ESRL profiler data from Appledore Island in conjunction with these trajectories. Thus the FLEXPART and profiler trajectories were used in a synergistic way to provide information on both longer-range and local-scale transport.

3. Results and Discussion

3.1. Classification of Samples by Regional Transport Sector

[20] Samples were classified into six major source regions on the basis of visual inspection of the column residence time, footprint residence plots and the archived HYSPLIT trajectories (Figure 2). There was only one 2 day period from 31 July to 1 August when the products disagreed significantly. In this case other meteorological products were examined, and the flow regime for this period was classified on the basis of the FLEXPART model only. In this classification, Northwesterly (NW) indicates typical post cold front flow, with the majority of trajectories indicating subsiding air. Midwest indicates transport from the west passing over or south of the Great Lakes region through large NO_x source regions. Southwest (SW) Urban indicates a source region to the southwest and includes trajectories that passed along the east coast urban corridor and may therefore also be marine-influenced. Air masses originating from the South (S) coastal direction likely passed along the Massachusetts coast, but not along the entire Eastern Seaboard. The Marine classification indicates easterly flow

Table 1. Summary Statistics for Gaseous HNO3 (N = 309 Excluding Data for Two Samples That Were Mishandled)

Statistic (N = 309)	pptv	nmol m^{-3}
10th percentile	186	8.3
25th percentile	302	13.5
Median	511	22.8
Mean	826	36.9
75th percentile	885	39.5
90th percentile	1825	81.5
Maximum	7546	337

off the ocean. Finally, the northern (N) New England and eastern Canada classification includes air masses that came from the north and passed over eastern New Hampshire, Maine and Quebec. This classification also includes trajectories that traveled from the northeast along the coast of Maine, and thus may also have been influenced by marine sources.

[21] Because of the short sampling intervals, each mist chamber sample was paired with one associated source region. With respect to the aerosol samples, nighttime samples were paired with PES plots/trajectories from 0000 to 0900 UTC, i.e., three plots at 3, 6, and 0900 UTC and two trajectories at 0000 and 0600 UTC. Daytime samples were paired with residence plots/trajectories from 0900 to 0000 UTC, i.e., five plots at 1200, 1500, 1800, 2100 and 0000 UTC, and three trajectories at 1200, 1800, and 0000 UTC. The overlap at the beginning and end of samples is because they were normally changed at about 0900 and about 0000 UTC. Aerosol samples were grouped by a predominant class if transport was consistent for >75% of the sampling interval, i.e., three consistent plots for nighttime samples and four consistent plots for daytime samples. This criterion allowed 44 of 60 aerosol samples to be classified into one individual transport regimes.

3.2. HNO$_3$

3.2.1. HNO$_3$ Median Concentration and Range

[22] The minimum, median and maximum concentrations of HNO$_3$ were <0.04, 22.8, and 337 nmol m^{-3} (<8, 504, and 7549 pptv), respectively (Table 1). *Dibb et al.* [2004] and *Keene et al.* [2004] measured HNO$_3$ on the *Ronald H. Brown* during NEAQS 2002. *Dibb et al.* [2004] measured HNO$_3$ with an automated dual mist chamber system over 5-min sampling intervals; *Keene et al.* [2004] used similar mist chamber techniques as in this study, with the exception noted above that the sampling inlets on Appledore Island were higher above the ocean surface (~43 m versus ~16 m aboard ship). For the portion of the cruse when the ship was in the region, maximum and median HNO$_3$ mixing ratios measured by *Dibb et al.* [2004] were 317 nmol m^{-3} (7100 pptv) and 36 nmol m^{-3} (810 pptv); the maximum HNO$_3$ mixing ratios at Appledore Island during 2004 was higher but the median concentration was lower than that measured in 2002 [*Dibb et al.*, 2004]. Data from *Keene et al.* [2004] was segregated by distance from Appledore Island. The minimum, median, and maximum concentrations of HNO$_3$ of the subset of data when the ship was within a 50 km radius of Appledore Island were 0.4, 22, and 287 nmol m^{-3} (93, 498, 6431 pptv).

[23] The median HNO$_3$ concentration measured on Appledore during ICARTT is comparable to those mea-

sured during summer 2000 at Lewes, Delaware (median = 22.5 nmol m^{-3}; 504 pptv) [*Russell et al.*, 2003], during summer 1997 at New Castle, New Hampshire (median = 21.4 nmol m^{-3}; 479 pptv), and during summers 1998 and 1999 at Clinton, North Carolina (median = ~20 nmol m^{-3}; 448 pptv) [*Robarge et al.*, 2002], but somewhat higher than those at Harvard Forest during summers 1991 to 1995 (median = 16.8 nmol m^{-3}; 376 pptv) [*Lefer et al.*, 1999].

3.2.2. HNO$_3$ Diurnal Cycle

[24] Nitric acid concentrations varied widely on the timescale of hours. However, all sampling days were characterized by a distinct minimum during the early morning hours, usually between 0900 and 1100 UTC (0500 and 0700 local time (LT)) (Figure 3). There were also days characterized by a distinct secondary minimum near sunset. The daily average minimum mixing ratio was 13.1 nmol m^{-3} (294 pptv). On average the increase in HNO$_3$ concentrations during the daytime exceeded 63 nmol m^{-3} (1.4 ppbv); on 3 days the concentration increased by ≥150 nmol m^{-3} (3340 nmol m^{-3}) from sunrise to midafternoon. These periods are discussed further in section 3.4. The daily peak HNO$_3$ concentration occurred anywhere from 1600 to 2300 UTC, but normally
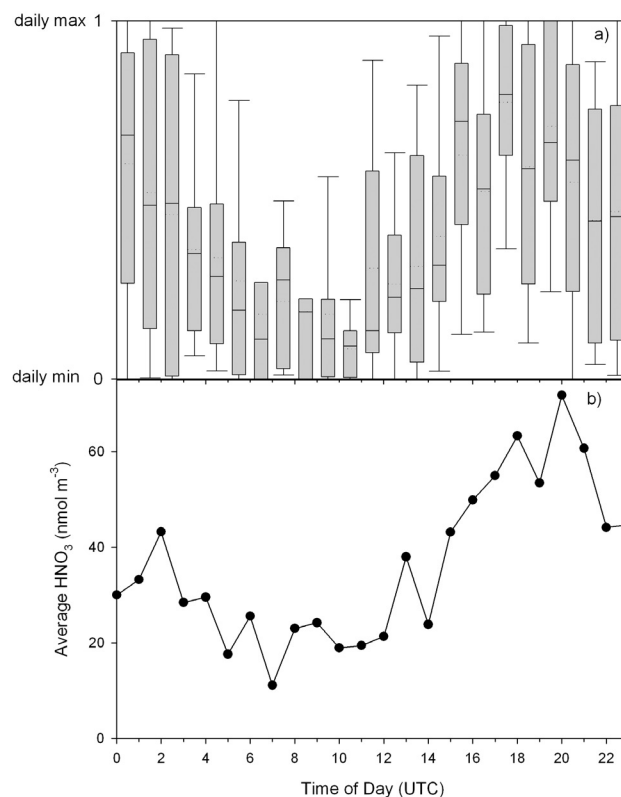
Figure 3. (a) Normalized HNO$_3$ diurnal cycle. In this plot the daily maximum HNO$_3$ concentration was set to 1 and the minimum concentration was set to 0. The dashed line represents the mean, and the solid line represents the median. The bottom of the box represents the 25th percentile and the top of the box represents the 75th percentile. The whiskers are the 10th and 90th percentiles. The same scheme holds for Figures 4 and 10. (b) Average HNO$_3$ diurnal cycle. The samples were segregated by their midpoint hour.
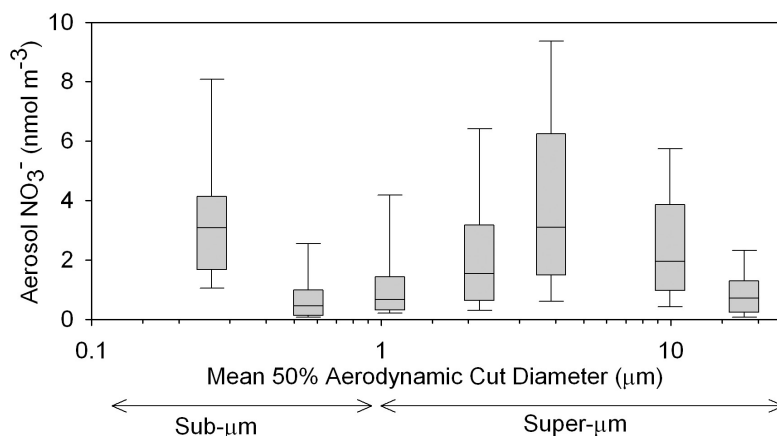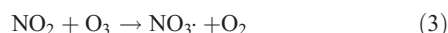
Figure 4. Aerosol NO_3^- size distribution. Sub-μm and super-μm NO_3^- indicates a sum of the inclusive impactor stages.

occurred in the early afternoon between 1800 and 2100 UTC (1200 and 1700 LT). Concentrations dropped rapidly after sunset, but the normalized and averaged diurnal cycles for the entire campaign (Figure 3), indicate a relative abundance of HNO_3 at night, which is consistent with a nocturnal HNO_3 source. Several nights during the campaign were marked by a distinct peak in HNO_3 between midnight and 0200 LT. The pronounced diurnal variation of HNO_3 can be attributed to photochemical production during the day via the following reaction [*McConnell and McElroy*, 1973]:

$$NO_2 + OH + M \rightarrow HNO_3 + M. \qquad (2)$$

Nighttime formation of the nitrate radical (NO_3) and dinitrogen pentoxide (N_2O_5) lead to HNO_3 production at night via this set of reactions:

$$NO_2 + O_3 \rightarrow NO_3\cdot + O_2 \qquad (3)$$

$$NO_3\cdot + NO_2 + M \rightarrow N_2O_5 + M \qquad (4)$$

$$N_2O_5 + H_2O \rightarrow 2HNO_3 \leftrightarrow 2H^+ + 2NO_3^- \qquad (5)$$

Reaction (5) is thought to occur primarily at aerosol surfaces. Reaction of $NO_3\cdot$ with hydrocarbons and reduced sulfur compounds can also produce HNO_3 at night [*Seinfeld and Pandis*, 1998]. Nighttime production accounts for about 35% of the total HNO_3 in the summertime MBL off the east coast of the United States, and the average nocturnal production rate of HNO_3 is roughly 80% of the average daytime production rate [*Brown et al.*, 2004].

[25] The major HNO_3 removal mechanisms are scavenging by aerosols (primarily the less acidic sea-salt aerosols) and dry and wet deposition. Model calculations suggest that ~50% of gaseous HNO_3 can be scavenged by sea-salt aerosols within an hour of mixing [*Erickson et al.*, 1999]. The early morning and evening minima in HNO_3 observed on Appledore during summer 2004 can be explained as the time when both the nighttime and daytime HNO_3 sources

are relatively weak. There is insufficient sunlight to drive photochemical OH production needed for reaction (2), but NO_3 concentrations are reduced because there is enough sunlight to photolyze NO_2 and suppress reaction (3) [*Brown et al.*, 2004]. The secondary minima near sunset were accompanied by clear increases in HNO_3 after sunset. There were six nights during the campaign characterized by pronounced nocturnal HNO_3 peaks: 12 July, 16 July, 18 July, 22 July, 28 July, and 5 August. This pattern was observed previously in the Gulf of Maine in 2002 by *Dibb et al.* [2004] and *Brown et al.* [2004]. J. L. Ambrose et al. (Nighttime nitrate radical chemistry at Appledore Island, ME during ICARTT 2004, submitted to *Journal of Geophysical Research*, 2006) provide an analysis of nighttime HNO_3 production based on parallel measurements of the nitrate radical (NO_3) and NO_2. Although nocturnal chemistry may represent a large NO_x sink, the number of previous studies addressing this issue is fairly limited.

3.3. Aerosol NO_3^-
3.3.1. Size Distribution
[26] Particulate NO_3^- exhibited a bimodal size distribution with a primary peak associated with sea salt at ~4 μm and a secondary sub-μm peak (Figure 4). The NO_3^- size distribution reflects the pH-dependent phase partitioning of HNO_3 with the aerosol solutions. The dissolution of HNO_3 into deliquesced sea-salt aerosols leads to the displacement of HCl into the gas phase [*Guimbaud et al.*, 2002]. During this campaign, displacement of HCl from sea-salt aerosol via incorporation of HNO_3 helped to sustain high mixing ratios of HCl (up to 255 nmol m^{-3}) and significant production of atomic Cl via HCl + OH during the daytime, thereby likely altering the oxidant regime relative to the upwind continent (see W. C. Keene et al., Inorganic chlorine and bromine in coastal New England air during summer, submitted to *Journal of Geophysical Research*, 2006).

[27] The bimodal NO_3^- size distribution was anticipated from results of previous measurement campaigns at New Castle, New Hampshire (located at the entrance to Portsmouth Harbor), and on the *Ronald H. Brown*, which indicated a predominant coarse fraction and a substantial sub-μm secondary peak that was most prominent under

Table 2. Summary Statistics for Aerosol NO_3^- [a]

	Stage									
Statistic	0 (18)	1 (9.9)	2 (3.9)	3 (2.2)	4 (1.1)	5 (0.56)	6	Sub-μm	Super-μm	Bulk
Maximum	2.73	10.0	14.6	8.27	4.92	4.09	19.0	19.1	39.3	79.0
Median	0.67	1.79	2.80	1.45	0.63	0.30	2.87	3.28	7.73	16.5
Mean	0.82	2.40	3.69	2.06	1.07	0.69	3.44	4.13	10.0	19.0
10th percentile	1.91	4.92	7.69	5.06	2.89	2.02	5.94	1.23	2.09	31.4
25th percentile	1.25	3.37	5.63	2.98	1.12	0.84	3.77	1.92	4.03	26.5
75th percentile	0.23	0.96	1.45	0.62	0.30	0.13	1.65	5.23	15.0	9.64
90th percentile	0.08	0.43	0.65	0.31	0.20	0.07	1.05	9.64	23.7	5.75

[a]All values are in nmol m^{-3}. The mean size for each impactor stage is given in parenthesis in μm. N = 60.

polluted continental flow [*Jordan et al.*, 2000]. Jordan et al. noted that the smaller secondary peak did not exist under onshore marine flow. The present data cannot confirm this because aerosol sampling was suspended during marine flow because of coincident precipitation. A similar size distribution was also noted during summer 2000 at Lewes [*Russell et al.*, 2003] and inland at Harvard Forest [*Lefer and Talbot*, 2001].

3.3.2. Median Concentration and Range

[28] Table 2 presents summary statistics for aerosol NO_3^-. The statistics presented in Table 2 were calculated separately for daytime and nighttime subsets of the data, and no obvious day-night differences were noted. The median concentration of aerosol NO_3^- for this campaign, 11 nmol m^{-3} (246 pptv) compares well with summertime measurements during the years 1994–1997 at New Castle (median = 7.9–11 nmol m^{-3}; 178–237 pptv) [*Jordan et al.*, 2000]. There was a smaller range in the concentrations of NO_3^- than that measured at Lewes by *Russell et al.* [2003] (range = 7.7–149 nmol m^{-3}; 172–3338 pptv) and the median concentration at Appledore was a factor of 2 lower (median = 33.1 nmol m^{-3}; 741 pptv). The median concentration measured at Appledore was a factor of 2 higher than summertime measurements made inland at Harvard Forest during summers 1991 to 1995 (median = 6.31 nmol m^{-3}; 237 pptv) [*Lefer and Talbot*, 2001].

3.4. Air Mass Origin and Phase Partitioning: Case Studies

[29] The highest concentrations of total nitrate were associated with transport from the heavily polluted Midwest and Southwest Urban source regions (Figures 5 and 6). Differences in HNO_3 phase partitioning between these sectors (primarily HNO_3 for the Midwest sector and relatively more NO_3^- for the Southwest Urban sector) reflect that sea-salt concentrations were a factor of ~3 higher during southwesterly flow. Transport from other, less polluted sectors exhibited relatively lower concentrations of total nitrate. Here we compare the chemical characteristics of air associated with transitions between westerly and southwesterly flow regimes to provide insight concerning controls on HNO_3 phase partitioning. We contrast three events with efficient transport of combustion products from the polluted SW Urban and Midwest source sectors primarily characterized by elevated HNO_3 followed by elevated NO_3^- with one event characterized by elevated aerosol NO_3^- and sustained low HNO_3.

[30] Event Type 1: The maximum HNO_3 mixing ratio (7546 pptv) was measured on 20 July. This marked the beginning of a multiday event which lasted from 20 to 22 July. Prior to the event air mass transport was from southerly and southeasterly directions. This was followed by a transition to westerly flow that carried peak HNO_3 mixing ratios. On 19 July a surface low-pressure system was centered over southern New England, with a midlevel trough axis positioned over the Great Lakes. On 20 July the surface low moved off the coast and the trough moved east. This situation created zonal flow aloft and generally southwesterly flow along the coast at lower altitudes, which coincided with an increase in the super-μm aerosol NO_3^-. The convergence of westerly winds aloft and southwesterly surface winds near Appledore suggests that this event resulted from a synergy of NO_x sources located upwind to the west and southwest.

[31] The second major HNO_3 event occurred from 30 to 31 July. From the afternoon of 29 to 30 July surface high pressure originally centered over Pennsylvania traveled east to the Gulf of Maine creating a relatively weak surface pressure gradient over the New England coastal region and southwesterly winds. Maximum land temperatures on the afternoon of 30 July hovered near 30°C, allowing a weak corkscrew sea breeze to develop in the early afternoon [*Miller et al.*, 2003]. A period of weak southerly winds over Appledore during this period provides evidence that the monitoring site was impacted by a mild sea breeze. By 31 July the surface isobars were organized parallel to the East Coast, which drove the transition to more rapid southwesterly flow. These conditions created a transition from westerly synoptic transport associated with relatively high concentrations of HNO_3 (280 nmol m^{-3}), relatively low concentrations of sea salt aerosol (28 nmol m^{-3} Na$^+$), and relatively low concentrations of super-μm NO_3^- (15 nmol m^{-3}) to southwesterly transport associated with lower concentrations of HNO_3 (<8.0–49 nmol m^{-3}) relatively higher sea salt concentrations (127 nmol m^{-3} Na$^+$), and relatively higher concentrations of super-μm NO_3^- (24 nmol m^{-3}) (Figures 7 and 8).

[32] A third major HNO_3 spike occurred on the afternoon of 3 August when HNO_3 reached 3894 pptv, and super-μm aerosol NO_3^- reached 20 nmol m^{-3} the following night. During this period a strong 500 mb trough was positioned over the Ohio River Valley, and at the surface a cold front was approaching western New England. Low-level winds shifted between southwesterly and westerly sectors and, similar to the other events, this event may have resulted
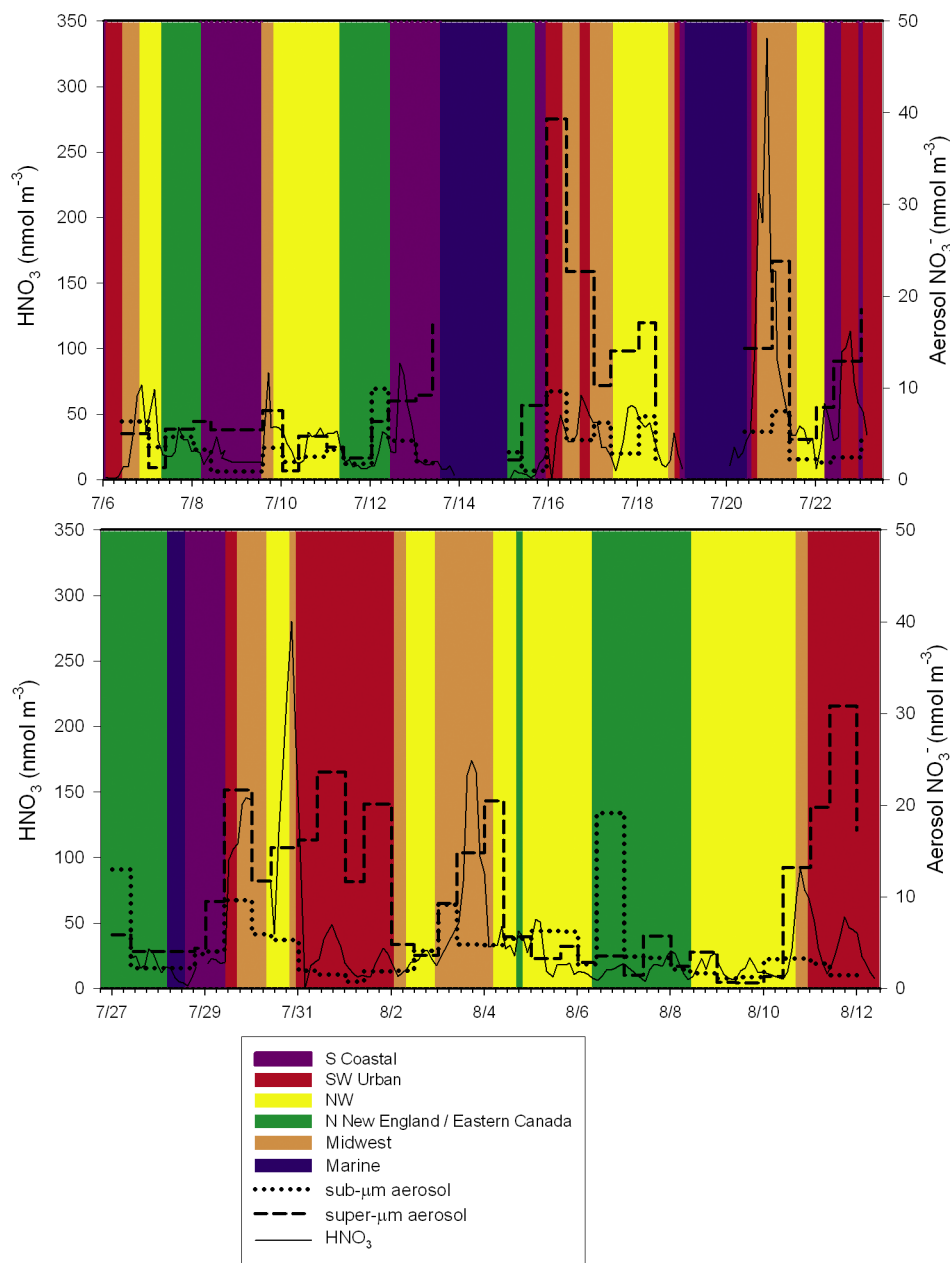
Figure 5. Time series of HNO_3 and aerosol NO_3^-. Note the different scales. The color scheme behind the time series represents the six major regions of influence identified in Figure 2. There was a 3-day break in sampling from 23 to 25 July.

from a synergy of NO_x sources located upwind to the west and southwest. Strong afternoon heating over land created favorable conditions for a sea breeze; however, a sea breeze was barely evident at Appledore Island. There was a short period where the low-level southwesterly winds transitioned to weaker southerly flow during the early afternoon.

[33] Event Type 2: In the early morning on 15 July low-level northeasterly winds resulted from a low-pressure system situated off Cape Cod. By midday this system weakened and moved further east; winds along the coast were then influenced by a low centered over Lake Ontario and shifted to southwesterly. During the afternoon a relatively strong sea breeze developed and was apparent in the

profiler data from Appledore Island; low-level southeasterly winds were observed from local noon (1600 UTC) to about 1900 LT (2300 UTC). After sunset southwesterly winds were observed at all levels above Appledore. These conditions coincided with the highest concentrations of sea-salt aerosol measured during the campaign (130 nmol m^{-3} Na$^+$) and relatively high concentrations of nss-SO_4^{2-} (193 nmol m^{-3}). In contrast to the events discussed above, the 15 July event (Figure 9) was characterized by sustained high sea salt concentrations prior to and throughout the event. Phase partitioning associated with the relatively higher sea-salt concentration during this period accounts for the sustained high concentrations of super-μm NO_3^- (39 nmol m^{-3}), and the relatively
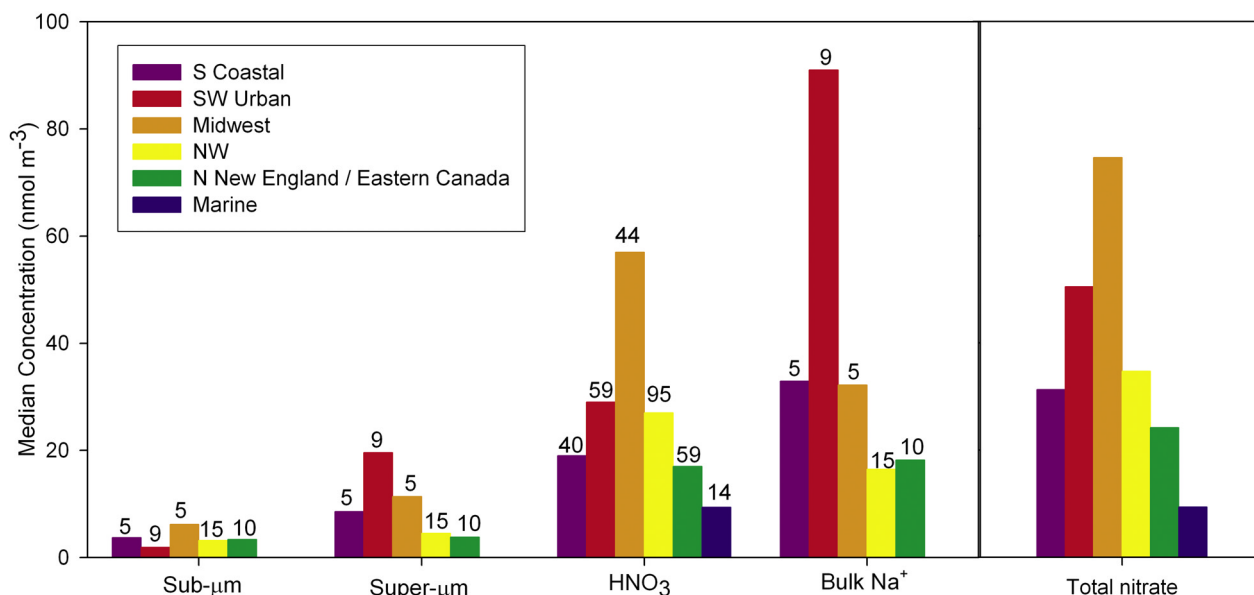
Figure 6. (left) Median concentration of aerosol sub- and super-μm NO_3^-, HNO_3, and bulk aerosol Na^+ by transport sector. (right) Sum of the median concentrations of sub- and super-μm NO_3^- and HNO_3 for each sector. Aerosol sampling was suspended during precipitation events, which often occurred under marine flow. Section 3.1.2 provides a detailed explanation of the sample classification. The numbers above each bar represent the number of samples in each classification.

low concentrations of HNO_3 ($3.1-64$ nmol m^{-3}) throughout the event. The peak super-μm NO_3^- concentrations occurred overnight on 16 July and were accompanied by a distinct nocturnal HNO_3 spike (49 nmol m^{-3}).

[34] An examination of the local profiler trajectories generally associated with southwesterly flow periods indicates that these air masses may have intercepted Cape Ann, MA within 1 or 2 hours before reaching Appledore Island; however, there was usually prior interaction with marine air farther upwind near Long Island, NY. Air masses traveling from the west leave the land near Portsmouth, New Hampshire, and arrive at Appledore in under an hour. When a sea breeze is not present or if there has not been recent easterly synoptic winds which have transported marine air inland, the amount of time during which there is an opportunity for the polluted continental air to mix with marine air under westerly transport is significantly less than during periods of southwesterly transport.

3.5. Dry Deposition Fluxes

[35] Modeled dry deposition of HNO_3 ranged from ~1 to 279 μmol m^{-2} d^{-1}, and dry deposition of aerosol NO_3^- ranged from ~1 to 43 μmol m^{-2} d^{-1} (Figure 10a). Because HNO_3 in coastal regions partitions preferentially with less acidic, sea-salt size fractions that exhibit high deposition velocities, super-μm particles dominated the dry-deposition of aerosol NO_3^- (Figure 10c). Modeled deposition velocities for the largest three size fractions were typically more than an order of magnitude larger than the modeled deposition velocities for the sub-μm stages. On average, the three largest size fractions contributed over 75% of the total NO_3^- aerosol flux. The two sub-μm stages normally contributed $\leq2\%$. An important point to draw from Figure 10 is that the modeled dry-deposition flux varied greatly during the campaign, with large fluxes occurring in sporadic pulses. These pulses reflect the interplay between meteorology and chemistry. First, modeled deposition velocities increase disproportionately with increasing wind velocity. Second, concentrations of total nitrate vary as a function of source region (Figure 6). Third, the phase partitioning (Figures 7 and 9) and modeled deposition velocities are a function of the sea-salt concentrations.
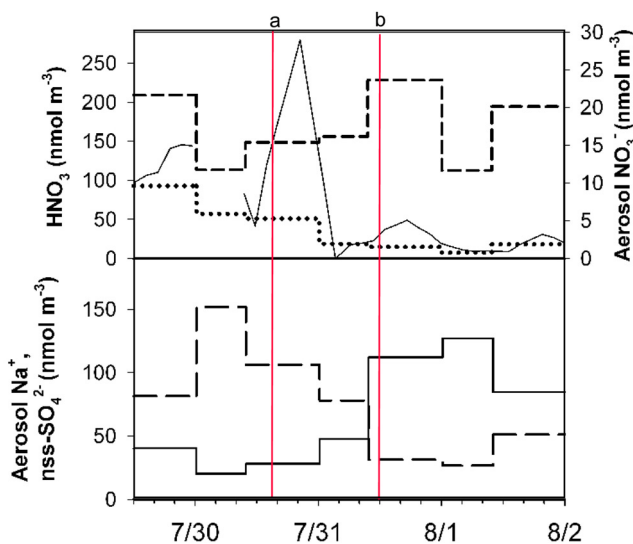

Figure 7. (top) Time series of HNO_3 (solid line), sub-μm (dotted line), and super-μm (dashed line) aerosol NO_3^-. (bottom) Time series of bulk Na^+ (solid line) and bulk non-sea-salt (nss) SO_4^{2-} (dashed line). The red lines correspond to the meteorology represented in Figure 8.
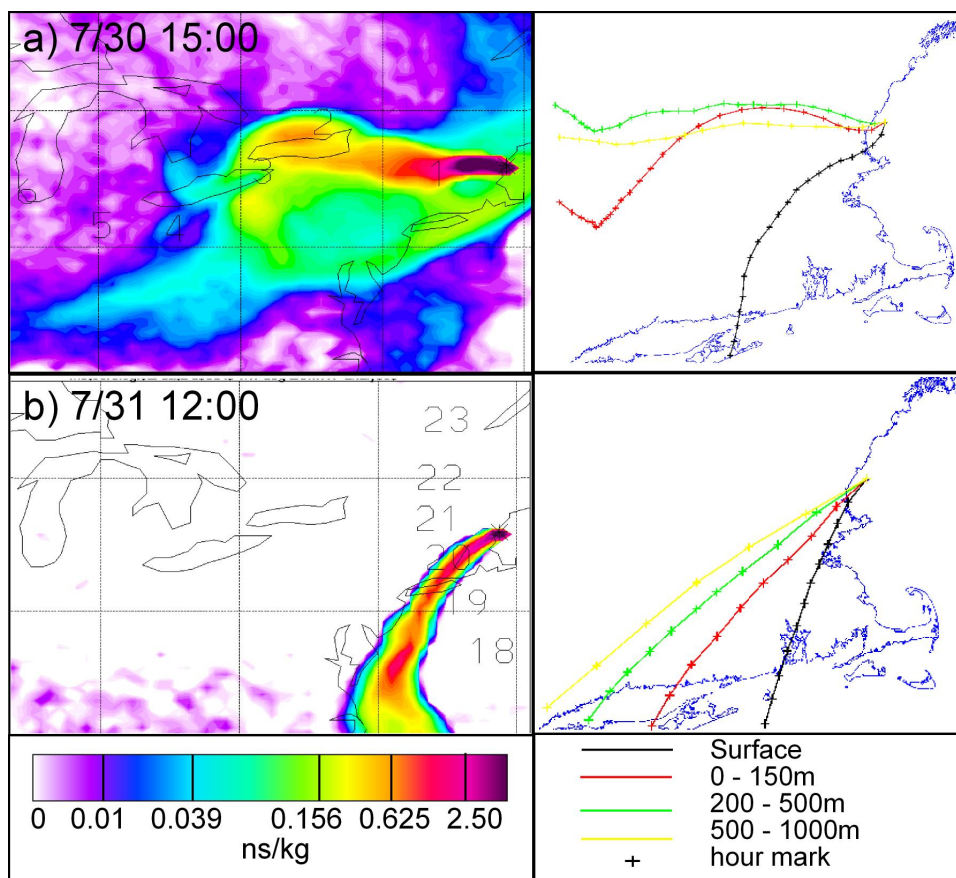
Figure 8. (left) Footprint PES plots for each time shown by the red bars in Figure 7. (right) The 36-hour backward trajectories based on local profiler and buoy data. Note the opportunity for multiple interactions with marine air during the period of southwesterly flow show in the bottom right trajectory plot. It is important to note that the surface trajectories (black) are invalidated immediately once they travel over land, especially during the daytime, as the air will not stay close to the ground.
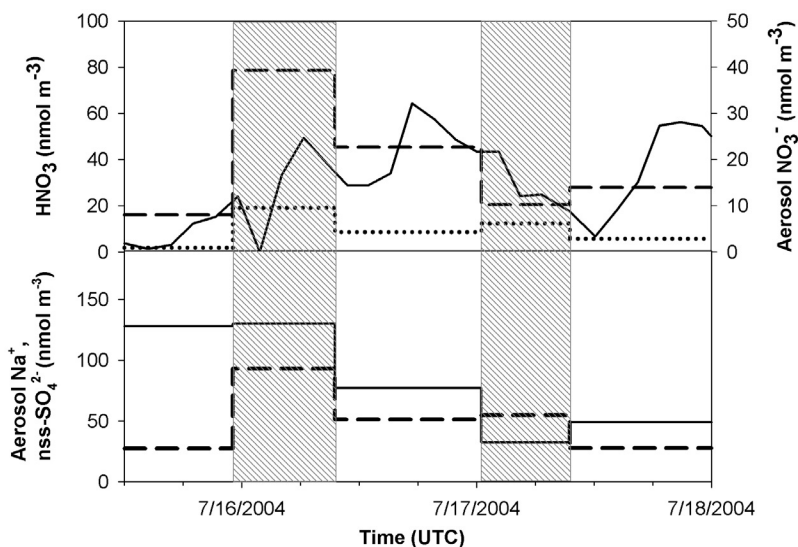

Figure 9. (top) Time series of HNO_3 (solid line), sub-μm (dotted line), and super-μm (dashed line) aerosol NO_3^- for the period 15 July 1200 UTC to 18 July 0000 UTC. (bottom) Time series of bulk Na^+ (solid line) and bulk non-sea-salt (nss) SO_4^{2-} (dashed line) for the same period. The shading indicates sunset to sunrise sampling periods.
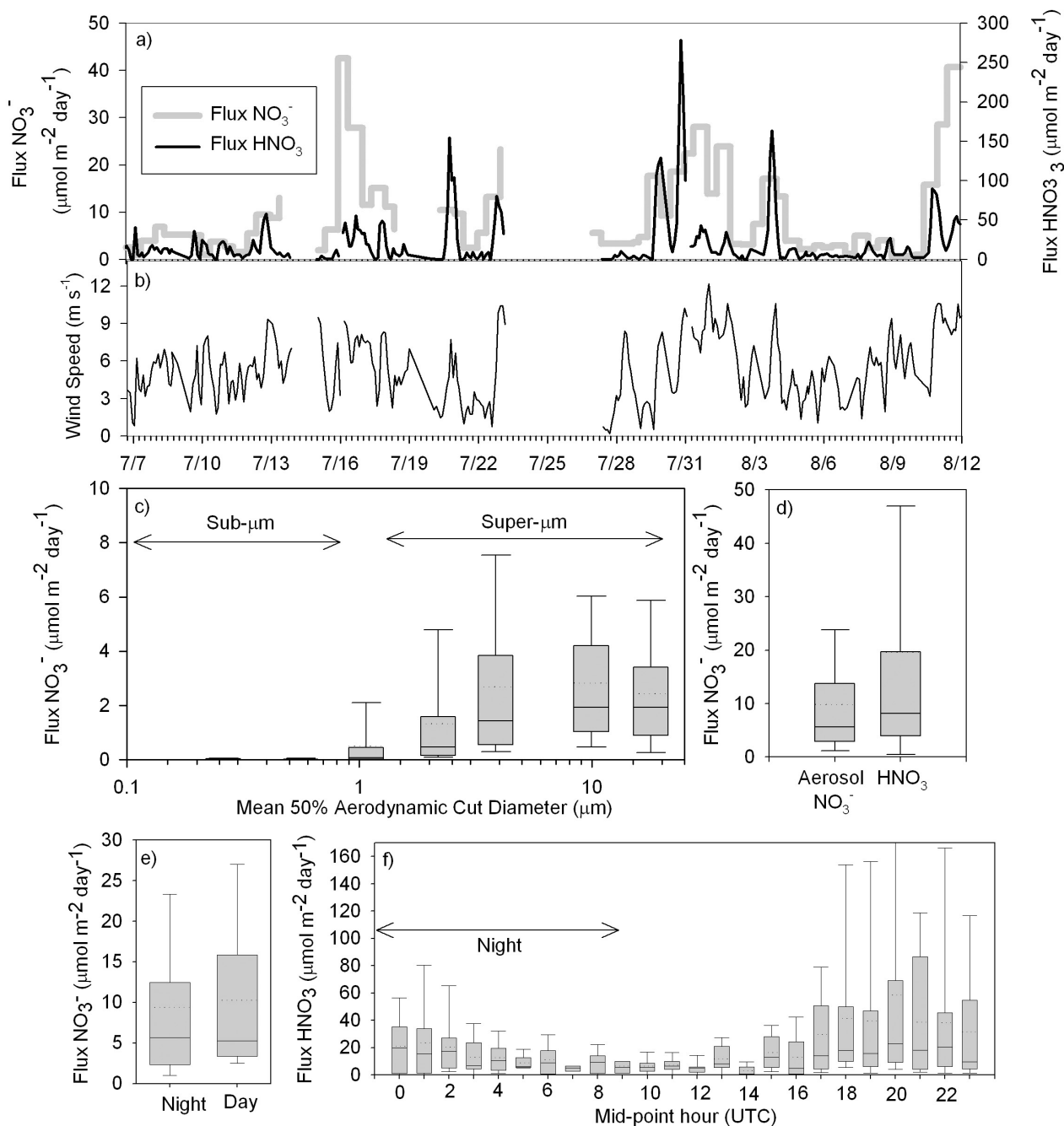
Figure 10. (a) Time series of total dry deposition flux from HNO_3 and aerosol NO_3^-. Note the different scales. Also note that HNO_3 samples were collected over 2-hour intervals. Large spikes in the HNO_3 flux may represent an elevated flux over a relatively short period of several hours. (b) Time series of mean wind speeds used to calculate HNO_3 dry deposition fluxes, (c) distribution of dry deposition flux by impactor stage, (d) distribution of dry deposition flux by phase, (e) distribution of the total aerosol NO_3^- dry deposition flux for night and day samples, and (f) diurnal cycle of the HNO_3 flux. The samples were segregated by their midpoint hour.

[36] Figure 10e and 10f provide information on the diurnal cycle of the dry-deposition flux. Figure 10e segregates the aerosol samples into daytime and nighttime subsets and shows the distribution of the dry deposition fluxes calculated for each sample. A Mann-Whitney U test indicated that means of the two subsets are not significantly different. However, the relatively long sampling duration limits the evaluation of diel variability in particulate NO_3^- concentrations and their associated dry-deposition fluxes. Dry deposition fluxes of HNO_3 peaked in the afternoon, at more than 11 $\mu mol\ m^{-2}\ hr^{-1}$ (Figure 10f). Median and mean values for the afternoon diverged substantially reflect-

Table 3. Median Dry Deposition Flux by Transport Sector[a]

Transport Sector	HNO$_3$		Total Aerosol NO$_3^-$		Median Wind Speed, m/s
	N	Median Flux, μmol m^{-2} d^{-1}	N	Median Flux, μmol m^{-2} d^{-1}	
S coastal	40	7.52	5	5.23	5.4
SW urban	59	21.7	9	23.9	8.8
Midwest	44	29.3	5	9.72	4.5
NW	95	6.02	15	2.74	4.3
N New England/eastern Canada	59	5.33	10	3.13	4.3
Marine	14	2.52	0	$\cdots$	5.9

[a]N indicates the number of samples that were classified to be predominantly associated with each sector as explained in section 3.1.2. Median wind speed was calculated using the wind speed values used to model the HNO$_3$ deposition.

ing the disproportionate influence of extreme values on the arithmetic averages. Large deposition pulses were infrequent, but made a major contribution to the overall deposition. The lowest deposition rates occurred in the early morning hours. This cycle parallels the HNO$_3$ diurnal cycle presented in Figure 3. Extrapolating the median for the campaign over the three month summer period yields a total deposition of nitrate to the coastal zone of $\sim$1.3 mmol m^{-2} for the months of June, July, and August; HNO$_3$ accounted for about 2/3 of the calculated deposition. For comparison the National Acid Deposition Program (NADP) reported $\sim$5 mmol m^{-2} (3.13 kg ha^{-1}) of wet NO$_3^-$ deposition during summer 2004 at the Casco Bay, Maine monitoring site (http://nadp.sws.uiuc.edu/ads/2004/ME96.pdf).

[37] The median concentration of total nitrate under the westerly transport regime (75 nmol m^{-3}) was higher than that for the southwesterly regime (51 nmol m^{-3}, Figure 6). However, HNO$_3$ dominated total nitrate during westerly flow whereas particulate NO$_3^-$ was relatively more important during periods of southwesterly flow because of the shift in phase partitioning associated with the higher sea salt. The shift in phase partitioning toward short-lived, super-μm particles coupled with somewhat higher wind velocities resulted in a substantially greater modeled median dry-deposition flux of total nitrate for southwesterly flow (Table 3). These results indicate that prolonged interaction times between polluted continental and sea salt aerosol in the coastal zone may increase the dry-deposition flux of total nitrate to New England coastal ecosystems.

[38] Modeled dry-deposition fluxes during this study were within the range of values reported by *Jordan and Talbot* [2000] on the basis of measurements made at a nearby coastal site over the course of several years (Table 4). Our results also indicate that the dry-deposition fluxes of total nitrate at Appledore Island during summer months are

slightly lower than those in the mid-Atlantic states [*Russell et al.*, 2003]. Finally, and as expected, dry-deposition fluxes of total nitrate along the U.S. mid-Atlantic and New England coastal zones are an order of magnitude greater than those reported for remote oceanic areas [*Talbot et al.*, 1986] [*Liu and Schwab*, 1987]; [*Pszenny*, 1987].

[39] The primary removal mechanism for NO$_x$ is oxidation to HNO$_3$, and subsequent wet or dry deposition (both gaseous and in association with particles) to the surface. In the Northeast during summer, approximately 45% of NO$_x$ emitted into the boundary layer each day is oxidized to HNO$_3$ and subsequently deposited to the surface [*Munger et al.*, 1998]. The lifetime of HNO$_3$ in the MBL in this region has been estimated to be 2.3 hours [*Brown et al.*, 2004].

[40] Total odd nitrogen (NO$_y$) is defined as the sum of all the gaseous inorganic nitrogen oxides: NO$_x$ + HNO$_3$ + PAN + HONO + HO$_2$NO$_2$ + NO$_3$ + 2N$_2$O$_5$ + other organic nitrogen-containing compounds. Chemical simulations indicate an export efficiency of anthropogenic NO$_y$ from North America of $\sim$20%, with a large contribution from NO$_x$ ($\sim$40%) [*Li et al.*, 2004]; but export varies significantly with altitude [*Stohl et al.*, 2002]. Using aircraft measurements along the western North Atlantic Ocean during spring 1996, *Stohl et al.* [2002] estimated that 33–76% of surface NO$_y$ emissions were lost within the boundary layer or during transport from it. *Stohl et al.* [2002] propose that the main removal mechanism is the dry deposition of HNO$_3$ in the boundary layer and the strong removal upon export from the boundary layer is due to washout, primarily of HNO$_3$. Efficient transport of HNO$_3$ and NO$_x$ is only possible in plumes that are above and largely decoupled from the MBL [*Neuman et al.*, 2006]. The nitrate dry deposition calculations summarized here provide a lower limit to the nitrate loss within the coastal MBL from North American continental air masses as they travel over coastal

Table 4. A Comparison of Dry Deposition Fluxes Estimated in This Study With Those Estimated in Previous Studies

Region	Aerosol NO$_3^-$, μmol m^{-2} d^{-1}	Volatile HNO$_3$, μmol m^{-2} d^{-1}	Reference
Appledore Island, Maine	median: 5.6, mean: 9.8	median: 8.2, mean: 19.7	this study
Mid-Atlantic US coast	mean: 11.0	mean: 35.1	*Russell et al.* [2003]
Gulf of Maine	$\cdots$	>11.2	*Dibb et al.* [2004]
New Castle, New Hampshire	median: 16 μmol N m^{-2} d^{-1} (HNO$_3$ + NO$_3^-$ + NH$_4^+$)	median: 16 μmol N m^{-2} d^{-1} (HNO$_3$ + NO$_3^-$ + NH$_4^+$)	*Jordan and Talbot* [2000]
Equatorial Pacific	mean: 1.0	0.45–1.8	*Liu et al.* [1983]
Tropical N Atlantic	mean: 1.5	$\cdots$	*Talbot et al.* [1986]
Tropical SW Pacific	mean: 0.56	0.14–1.4	*Pszenny* [1987]
Temperate SW Pacific	mean: 0.66	0.13–0.64	*Pszenny* [1987]

ecosystems en route to the North Atlantic marine atmosphere, and confirm that during periods of southwesterly and westerly transport the coastal MBL is a significant HNO_3 sink.

4. Summary

[41] Gaseous HNO_3 and size-resolved particulate NO_3^- were measured in the MBL at Appledore Island, Maine, between 6 July and 12 August 2004. HNO_3 concentrations varied widely on the timescale of hours; however, most days were characterized by minima at dawn and maxima during the afternoon: maximum, median and minimum concentrations of HNO_3 during the campaign were 337, 22.5, and 0.04 nmol m^{-3}, respectively. Aerosol NO_3^- exhibited a bimodal size distribution with a primary peak associated with sea-salt at $\sim$4 μm and a secondary sub-μm peak. The median NO_3^- concentrations in sub- and super-μm diameter size fractions were 3.3 and 7.7 nmol m^{-3}, respectively.

[42] The multiphase cycling of HNO_3 was evaluated as a function of transport sector. Peak HNO_3 concentrations were associated with westerly flow, while super-μm aerosol peaked during southwesterly flow. The phase partitioning of HNO_3 varied as a function of transportation and sea-salt concentration; sea-salt concentrations were a factor of $\sim$3 higher during southwesterly flow relative to westerly flow. Transport from other, less polluted sectors, exhibited relatively lower concentrations of total nitrate.

[43] Modeled dry-deposition fluxes for HNO_3 varied over two orders of magnitude, and the largest fluxes were during the afternoon coincident with the highest concentrations. Because HNO_3 in coastal regions partitions preferentially with less acidic, sea-salt size fractions that exhibit high deposition velocities, super-μm particles dominated the dry-deposition of aerosol NO_3^-. Modeled dry deposition of HNO_3 ranged from $\sim$1 to 279 μmol m^{-2} d^{-1}, and dry deposition of aerosol NO_3^- ranged from $\sim$1 to 43 μmol m^{-2} d^{-1}. On the basis of these results, there was a modest enhancement of total nitrate dry-deposition to the coastal ecosystem near Appledore Island when polluted continental air traveled along the coast for $\geq$1 hour. Atmospheric dry-deposition contributes a minor amount to the total nitrogen input to the Gulf of Maine on an annual basis and is a factor of $\sim$5 less than estimates of wet deposition. However, results of the present study indicate that during summer months the dry deposition flux to the coastal ecosystem is highly episodic, allowing the possibility that atmospheric deposition of reactive nitrogen to this zone may play an important role on an event basis.

References

Angevine, W. M., M. P. Buhr, J. S. Holloway, M. Trainer, D. D. Parrish, J. I. MacPherson, G. L. Kok, R. D. Schillawski, and D. H. Bowlby (1996a), Local meteorological features affecting chemical measurements at a North Atlantic coastal site, *J. Geophys. Res.*, *101*(D22), 28,935–28,946.

Angevine, W. M., M. Trainer, S. A. McKeen, and C. M. Berkowitz (1996b), Mesoscale meteorology of the New England coast, Gulf of Maine, and Nova Scotia: Overview, *J. Geophys. Res.*, *101*(D22), 28,893–28,901.

Angevine, W. M., C. Fairall, D. Wolfe, J. Hare, and C. J. Senff (2005), Structure and formation of the highly stable marine boundary layer over the Gulf of Maine, *Eos Trans. AGU*, *86*(52), Fall Meet. Suppl., Abstract A31A-0804.

Bisagni, J. J. (2003), Seasonal variability of nitrate supply and potential new production in the Gulf of Maine and Georges Bank regions, *J. Geophys. Res.*, *108*(C11), 8015, doi:10.1029/2001JC001136.

Brooks, D. A. (1985), Vernal circulation in the Gulf of Maine, *J. Geophys. Res.*, *90*, 4687–4705.

Brown, S. S., et al. (2004), Nighttime removal of NO_x in the summer marine boundary layer, *Geophys. Res. Lett.*, *31*, L07108, doi:10.1029/2004GL019412.

Castro, M. S., C. T. Driscoll, T. E. Jordan, W. G. Reay, W. R. Boynton, S. P. Seitzinger, R. V. Styles, and J. E. Cable (2001), Contribution of atmospheric deposition to the total nitrogen loads to thirty-four estuaries on the Atlantic and Gulf coasts of the United States, in *Nitrogen Loading in Coastal Water Bodies: An Atmospheric Perspective, Coastal Estuarine Stud.*, vol. 57, edited by pp. 77–106, AGU, Washington, D. C.

Dibb, J. E., E. Scheuer, S. I. Whitlow, M. Vozella, E. Williams, and B. M. Lerner (2004), Ship-based nitric acid measurements in the Gulf of Maine during New England Air Quality Study 2002, *J. Geophys. Res.*, *109*, D20303, doi:10.1029/2004JD004843.

Draxler, R. R., and G. D. Rolph (2005), HYSPLIT (Hybrid Single-Particle Lagrangian Integrated Trajectory) model access via NOAA ARL READY, NOAA Air Resour. Lab., Silver Spring, Md. (Available at http://www.arl.noaa.gov/ready/hysplit4.html)

Driscoll, C. T., et al. (2003), Nitrogen pollution in the northeastern United States: Sources, effects, and management options, *Biosci.*, *53*(4), 357–374.

Erickson, D. J., III, C. Seuzaret, W. C. Keene, and S. L. Gong (1999), A general circulation model based calculation of HCl and $ClNO_2$ production from sea salt dechlorination: Reactive Chlorine Emissions Inventory, *J. Geophys. Res.*, *104*(D7), 8347–8372.

Frost, G. J., et al. (2006), Effects of changing power plant NO_x emissions on ozone in the eastern United States: Proof of concept, *J. Geophys. Res.*, *111*, D12306, doi:10.1029/2005JD006354.

Galloway, J. N., and E. B. Cowling (2002), Reactive nitrogen and the world: 200 years of change, *Ambio*, *31*(2), 64–71.

Guimbaud, C., F. Arens, L. Gutzwiller, H. W. Gaggeler, and M. Ammann (2002), Uptake of HNO_3 to deliquescent sea-salt particles, *Atmos. Chem. Phys. Disc.*, *2*, 739–763.

Hicks, B. B. (1975), A procedure for the formulation of bulk transfer coefficients over water, *Boundary Layer Meteorol.*, *8*, 515–524.

Hummelshoj, N. O., N. O. Jensen, and S. E. Larsen (1992), Particle dry deposition to a sea surface, in *Precipitation Scavenging and Atmosphere-Surface Exchange*, pp. 829–840, Taylor and Francis, Philadelphia, Pa.

Jordan, C. E., and R. W. Talbot (2000), Direct atmospheric deposition of water-soluble nitrogen to the Gulf of Maine, *Global Biogeochem. Cycles*, *14*(4), 1315–1329.

Jordan, C. E., R. W. Talbot, and B. D. Keim (2000), Water-soluble nitrogen at the New Hampshire sea coast: HNO_3, aerosols, precipitation, and fog, *J. Geophys. Res.*, *105*(D21), 26,403–26,431.

Keene, W. C., A. A. P. Pszenny, J. N. Galloway, and M. E. Hawley (1986), Sea-salt corrections and interpretation of constituent ratios in marine precipitation, *J. Geophys. Res.*, *91*, 6647–6658.

Keene, W. C., et al. (1989), An intercomparison of measurement systems for vapor and particulate phase concentrations of formic and acetic acids, *J. Geophys. Res.*, *94*(D5), 6457–6471.

Keene, W. C., A. A. P. Pszenny, D. J. Jacob, R. A. Duce, J. N. Galloway, J. J. Schultz-Tokos, H. Sievering, and J. F. Boatman (1990), The geochemical cycling of reactive chlorine through the marine troposphere, *Global Biogeochem. Cycles*, *4*, 407–430.

Keene, W. C., J. R. Maben, A. A. P. Pszenny, and J. N. Galloway (1993), Measurement techniques for inorganic chlorine gases in the marine boundary layer, *Environ. Sci. Technol.*, *27*, 866–874.

Keene, W. C., A. A. P. Pszenny, J. R. Maben, E. Stevenson, and A. Wall (2004), Closure evaluation of size-resolved aerosol pH in the New England coastal atmosphere during summer, *J. Geophys. Res.*, *109*, D23307, doi:10.1029/2004JD004801.

Lefer, B. L., and R. W. Talbot (2001), Summertime measurements of aerosol nitrate and ammonium at a northeastern U.S. site, *J. Geophys. Res.*, *106*(D17), 20,365–20,378.

Lefer, B. L., R. W. Talbot, and J. W. Munger (1999), Nitric acid and ammonia at a rural northeastern U.S. site, *J. Geophys. Res.*, *104*(D1), 1645–1661.

Lewis, E. R., and S. E. Schwartz (2004), *Sea Salt Aerosol Production: Mechanisms, Methods, Measurements, and Models*, Geophys. Monogr. Ser., vol. 152, AGU, Washington, D. C.

Li, Q., D. J. Jacob, J. W. Munger, R. M. Yantosca, and D. D. Parrish (2004), Export of NOy from the North American boundary layer: Reconciling aircraft observations and global model budgets, *J. Geophys. Res.*, 109, D02313, doi:10.1029/2003JD004086.

Liu, P. C., and D. J. Schwab (1987), A comparison of methods for estimating u* from given uz and air-sea temperature differences, *J. Geophys. Res.*, 92(C6), 6488–6494.

Liu, S. C., M. McFarland, D. Kley, O. Zafiriou, and B. Huebert (1983), Tropospheric NOx and O3 budgets in the equatorial Pacific, *J. Geophys. Res.*, 88, 10,785–10,807.

McConnell, J. C., and M. B. McElroy (1973), Odd nitrogen in the atmosphere, *J. Atmos. Sci.*, 30(8), 1465–1480.

Miller, S. T. K., and B. D. Keim (2003), Synoptic-scale controls on the sea breeze of the central New England coast, *Weather Forecasting*, 18, 236–248.

Miller, S. T. K., B. D. Keim, R. W. Talbot, and H. Mao (2003), Sea breeze: Structure, forecasting, and impacts, *Rev. Geophys.*, 41(3), 1011, doi:10.1029/2003RG000124.

Moody, J. L., J. W. Munger, A. H. Goldstein, D. J. Jacob, and S. C. Wofsy (1998), Harvard Forest regional-scale air mass composition by Patterns in Atmospheric Transport History (PATH), *J. Geophys. Res.*, 103, 13,181–13,194.

Munger, J. W., S. Fan, P. S. Bakwin, M. L. Goulden, A. H. Goldstein, A. S. Colman, and S. C. Wofsy (1998), Regional budgets for nitrogen oxides from continental sources: Variations of rates for oxidation and deposition with season and distance from source regions, *J. Geophys. Res.*, 103(D7), 8355–8368.

Neuman, J. A., et al. (2006), Reactive nitrogen transport and photochemistry in urban plumes over the North Atlantic Ocean, *J. Geophys. Res.*, 111, D23S54, doi:10.1029/2005JD007010.

Owens, N. J. P., J. N. Galloway, and R. A. Duce (1992), Episodic atmospheric nitrogen deposition to oligotrophic oceans, *Nature*, 357, 397–399.

Paerl, H. W. (1988), Nuisance phytoplankton blooms in coastal, estuarine, and inland waters, *Limnol. Oceanogr.*, 33, 823–847.

Paerl, H. W. (1997), Coastal eutrophication and harmful algal blooms: Importance of atmospheric deposition and groundwater at "new" nitrogen and other nutrient sources, *Limnol. Oceanogr.*, 42(5), part 2, 1154–1165.

Paerl, H. W., and D. R. Witall (1999), Anthropogenically-derived atmospheric nitrogen deposition, marine eutrophication and harmful algal bloom expansion: Is there a link?, *Ambio*, 28(4), 307–311.

Pszenny, A. A. P. (1987), Atmospheric deposition of nitrate to the ocean surface, Ph.D. thesis, 269 pp., Univ. of R. I., Kingston.

Ray, J. D., R. L. Heavner, M. Flores, and C. W. Michaealson (1996), Surface level measurements of ozone and precursors at coastal and offshore locations in the Gulf of Maine, *J. Geophys. Res.*, 101(D22), 29,005–29,011.

Robarge, W. P., J. T. Walker, R. B. McCulloh, and G. Murray (2002), Atmospheric concentrations of ammonia and ammonium at an agricultural site in the southeast United States, *Atmos. Environ.*, 36, 1661–1674.

Russell, K. M., W. C. Keene, J. R. Maben, J. N. Galloway, and J. L. Moody (2003), Phase partitioning and dry deposition of atmospheric nitrogen at the mid-Atlantic U.S. coast, *J. Geophys. Res.*, 108(D21), 4656, doi:10.1029/2003JD003736.

Schlitz, R. J., and E. B. Cohen (1984), A nitrogen budget for the Gulf of Maine and Georges Bank, *Biol. Oceanogr.*, 2, 203–222.

Seibert, P., and A. Frank (2004), Source-receptor matrix calculation with a Lagrangian particle dispersion model in backward mode, *Atmos. Chem. Phys.*, 4, 51–63.

Seinfeld, J. H., and S. N. Pandis (1998), *Atmospheric Chemistry and Physics: From Air Pollution to Climate Change*, John Wiley, Hoboken, N. J.

Senff, C. J., et al. (2005), Vertical structure, transport, and mixing of ozone and aerosols observed during NEAQS/ICARTT 2004, *Eos Trans. AGU*, 86(52), Fall Meet. Suppl., Abstract A53D-08.

Stohl, A., M. Hittenberger, and G. Wotawa (1998), Validation of the Lagrangian particle dispersion model FLEXPART against large scale tracer experiment data, *Atmos. Environ.*, 32, 4245–4264.

Stohl, A., M. Trainer, T. B. Ryerson, J. S. Holloway, and D. D. Parrish (2002), Export of NOy from the North American boundary layer during 1996 and 1997 North Atlantic Regional Experiments, *J. Geophys. Res.*, 107(D11), 4131, doi:10.1029/2001JD000519.

Stohl, A., C. Forster, S. Eckhardt, N. Spichtinger, H. Huntrieser, J. Heland, H. Schlager, S. Wilhelm, F. Arnold, and O. Cooper (2003), A backward modeling study of intercontinental pollution transport using aircraft measurements, *J. Geophys. Res.*, 108(D12), 4370, doi:10.1029/2002JD002862.

Stohl, A., C. Forster, A. Frank, P. Seibert, and G. Wotawa (2005), Technical note: The Lagrangian particle dispersion model FLEXPART version 6.2, *Atmos. Chem. Phys.*, 5, 2461–2474.

Stolte, W., T. McCollin, A. Noordeloos, and R. Riegman (1994), Effects of nitrogen source on the size distribution within marine phytoplankton populations, *J. Exp. Mar. Biol.*, 184, 83–97.

Talbot, R. W., R. C. Harriss, E. V. Browell, G. L. Gregory, D. I. Setacher, and S. M. Beck (1986), Distribution and geochemistry of aerosols in the tropical North Atlantic troposphere: Relationship to Saharan dust, *J. Geophys. Res.*, 91, 5173–5182.

Townsend, D. W. (1998), Sources and cycling of nitrogen in the Gulf of Maine, *J. Mar. Syst.*, 16, 283–295.

U.S. Environmental Protection Agency (2002), Sources of hydrocarbon and NOx emissions in New England, Boston, Mass. (http://www.epa.gov/region01/airquality/piechart.html)

Valigura, R. A. (1995), Iterative bulk exchange model for estimating air-water transfer of HNO3, *J. Geophys. Res.*, 100(D12), 26,045–26,050.

Willeke, K. (1975), Performance of the slotted impactor, *Am. Ind. Hygene Assoc. J.*, 36, 683–691.

————————

E. Fischer and A. Pszenny, Mount Washington Observatory, 2779 White Mountain Highway, P.O. Box 2310, North Conway, NH 03860, USA. (efischer@mountwashington.org)

W. Keene, J. Maben, and A. Smith, Department of Environmental Sciences, University of Virginia, Charlottesville, VA 22904, USA.

A. Stohl, Norwegian Institute for Air Research, N-2027 Kjeller, Norway.

R. Talbot, Institute for the Study of Earth, Oceans, and Space, University of New Hampshire, Durham, NH 03824, USA.